Marquette University
e-Publications@Marquette

Biological Sciences Faculty Research and Publications

Biological Sciences, Department of

9-1-2015

The Tumor Suppressor HHEX Inhibits Axon Growth when Prematurely Expressed in Developing Central Nervous System Neurons

Matthew T. Simpson
Marquette University

Ishwariya Venkatesh
Marquette University

Ben L. Callif
Marquette University

Laura K. Thiel
Marquette University

Denise M. Coley
Marquette University

See next page for additional authors

Authors

Matthew T. Simpson, Ishwariya Venkatesh, Ben L. Callif, Laura K. Thiel, Denise M. Coley, Kristen N. Winsor, Zimei Wang, Audra A. Kramer, Jessica K. Lerch, and Murray G. Blackmore

The Tumor Suppressor HHEX Inhibits Axon Growth When Prematurely Expressed in Developing Central Nervous System Neurons

Matthew T. Simpson

Department of Biomedical Sciences, Marquette University
Milwaukee, WI

Ishwariya Venkatesh

Department of Biomedical Sciences, Marquette University
Milwaukee, WI

Ben L. Callif

Department of Biomedical Sciences, Marquette University
Milwaukee, WI

Laura K. Thiel

Department of Biomedical Sciences, Marquette University
Milwaukee, WI

Denise M. Coley

Department of Biomedical Sciences, Marquette University
Milwaukee, WI

Kristen N. Winsor

Department of Biomedical Sciences, Marquette University
Milwaukee, WI

Zimei Wang

Department of Biomedical Sciences, Marquette University
Milwaukee, WI

Audra A. Kramer

Department of Biomedical Sciences, Marquette University
Milwaukee, WI

Jessica K. Lerch

The Center for Brain and Spinal Cord Repair,
The Department of Neuroscience, The Ohio State University,
Columbus, OH

Murray G. Blackmore

Department of Biomedical Sciences, Marquette University
Milwaukee, WI

Abstract: Neurons in the embryonic and peripheral nervous system respond to injury by activating transcriptional programs supportive of axon growth, ultimately resulting in functional recovery. In contrast, neurons in the adult central nervous system (CNS) possess a limited capacity to regenerate axons after injury, fundamentally constraining repair. Activating pro-regenerative gene expression in CNS neurons is a promising therapeutic approach, but progress is hampered by incomplete knowledge of the relevant transcription factors. An emerging hypothesis is that factors implicated in cellular growth and motility outside the nervous system may also control axon growth in neurons. We therefore tested sixty-nine transcription factors, previously identified as possessing tumor suppressive or oncogenic properties in non-neuronal cells, in assays of neurite outgrowth. This screen identified YAP1 and E2F1 as enhancers of neurite outgrowth, and PITX1, RBM14, ZBTB16, and HHEX as inhibitors. Follow-up experiments are focused on the tumor suppressor HHEX, one of the strongest growth inhibitors. HHEX is widely expressed in adult CNS neurons, including corticospinal tract neurons after spinal injury, but is present only in trace amounts in immature cortical neurons and adult peripheral neurons. HHEX overexpression in early postnatal cortical neurons reduced both initial axonogenesis and the rate of axon elongation, and domain deletion analysis strongly implicated transcriptional repression as the underlying mechanism. These findings suggest a role for HHEX in restricting axon growth in the developing CNS, and substantiate the

hypothesis that previously identified oncogenes and tumor suppressors can play conserved roles in axon extension.

Keywords: Axon regeneration, Transcription factor, High content screening

1. Introduction

In contrast to the peripheral nervous system (PNS) and the developing central nervous system (CNS), axons in the mature CNS generally fail to regenerate after injury. While external inhibitory factors contribute (Case and Tessier-Lavigne, 2005; Yiu and He, 2006), a major reason for regenerative failure is a loss of growth ability that is intrinsic to CNS neurons (Goldberg et al., 2002, Blackmore and Letourneau, 2006 and Sun and He, 2010). Intervening in the CNS cell body response, either by increasing pro-regenerative gene expression or eliminating growth-inhibitory gene expression, has emerged as a promising strategy to promote axon growth (Park et al., 2008, Moore et al., 2009, Liu et al., 2010b and Blackmore et al., 2012). Given the substantial amount and diversity of cellular material needed for axon growth, it is probable that multiple targets must be altered for optimal regeneration (Sun et al., 2011). Thus transcription factors (TFs), which coordinate the expression of multiple genes, are well suited to have a profound effect on axonal growth (Moore and Goldberg, 2011 and Patodia and Raivich, 2012). A number of TFs have been identified that regulate axon regeneration, but our understanding remains incomplete and additional transcriptional regulators of axon growth almost certainly await discovery (Moore and Goldberg, 2011).

It has been proposed that cellular growth mechanisms present in replicating cells outside the nervous system are conserved in post-mitotic neurons and may play key roles in axon growth (Park et al., 2008). Tumor-suppressive factors that prevent aberrant proliferation in dividing cells may act to restrict axon growth in neurons, whereas factors with oncogenic properties may act to promote axon growth (Pomerantz and Blau, 2013). Supporting this concept, signaling pathways involved in cancer progression have been found to affect neurite outgrowth (Buchser et al., 2010), most notably the mTOR pathway (Park et al., 2008) and the oncogene MYC (Belin et al., 2015). Furthermore, TFs such as KLF family members and Sox11, shown recently to promote CNS axon regeneration, are also well-

studied in cancer biology ([Blackmore et al., 2012](#) and [Wang et al., 2015](#)). These findings suggest that additional transcription factors, identified previously as displaying oncogenic or tumor suppressive properties in mitotically active cells, may regulate axon extension in neurons.

To test this hypothesis we adopted a high content screening strategy in which 69 TFs, implicated previously in cancer progression, were overexpressed in assays of neurite outgrowth. Nine of these TFs were found to significantly alter neurite length, of which a tumor suppressor called Hematopoietically Expressed [Homeobox](#) ([HHEX](#)) was among the most consistent and potent growth inhibitors. In follow-up experiments we confirmed strong suppression of axon growth by HHEX without a corresponding decrease in cell viability. Moreover, although HHEX has previously been described only in non-neuronal tissues, we show expression of HHEX in the CNS that is widespread and specific to neurons. In contrast we detected only low levels of HHEX in early postnatal CNS and adult PNS neurons, and found that forced elevation of HHEX expression reduces axon growth ability. Overall these data substantiate the mechanistic link between axon growth and general cellular growth at the level of transcriptional control, and suggest that the tumor suppressor HHEX may function as a novel transcriptional inhibitor of axon growth in the CNS.

2. Methods

2.1. Cloning and plasmid preparation

For screening and cell viability experiments, DNA was prepared (QIAprep Spin Miniprep Kit, Qiagen 27106) from [glycerol](#) stocks of NIH Mammalian Genome Collection in pSPORT6-CMV expression vectors (Open Biosystems, ThermoFisher, Huntsville, Alabama) ([Gerhard et al., 2004](#)). To create constructs for domain mutation analysis, a CAMKIIa promoter sequence (([Zhang et al., 2007](#)), Addgene #20944)) replaced the original CMV in pAAV-[EBFP](#)-2A-mCherry backbone (described previously, ([Blackmore et al., 2012](#))), generating pAAV-CAMKIIa-EBFP-2A-mCherry. Next, a Histone-2B sequence (([Kita-Matsuo et al., 2009](#)) (Addgene #21217)) was inserted 5' to mCherry. cDNA encoding human [HHEX](#) (Accession BC050638) was purchased

from Open Biosystems. The open reading frame (aa 1–270) was PCR-amplified and used to replace EBFP, creating CAMKIIa-HHEX-2A-H2B-mCherry. To create additional constructs, full length HHEX was replaced with amino acids 137–270 (Homeodomain and Activation domain, HHEX-ΔN), HHEX-ΔN fused to an Engrailed domain, as described in Blackmore et al. (2012), or amino acids 1–210 (repression domain and homeodomain, HHEX-ΔC). DNA was prepared by EndoFree Plasmid Maxi Kit (Qiagen 12362) and diluted to 1 µg/µl in endotoxin-free TE buffer.

2.2. Cortical cell dissociation, transfection, and culture

All animal procedures were approved by the Marquette University Institutional Animal Care and Use Committee. Cortical neurons were prepared from Sprague Dawley rat pups (Harlan) and transfected as in Blackmore et al. (2010). Briefly, early postnatal (P3–P5) frontal cortices were placed in ice-cold Hibernate E (Life Technologies A12476-01), their meninges removed, minced finely and transferred into 10 ml dissociation media for 30 min at 37 °C with constant shaking (HibernateE containing 20 U/ml papain (Worthington 3126) and 2.5 µg/ml DNAse (Sigma D4527)). Cells were then rinsed with Hibernate E + 2% SM1, gently triturated three times, rinsed in Hibernate E (no SM1), and incubated 30 min at 37 °C with constant shaking in 10 ml trypsin solution (Hibernate E containing 0.25% trypsin (Invitrogen/Gibco 15,090–046) and 2.5 µg/ml DNAse (Sigma D4527)). Cells were pelleted, washed with Hibernate E + 2% SM1, and triturated three times in 1.5 ml Hibernate E + 2% SM1 containing 2 µl DNAse (Sigma D4527). The suspension settled for 2 min and the supernatant was collected; the process was repeated until no cell clumps were visible. Collected cells were washed and resuspended in 6-7 ml Hibernate E, typically yielding 2 million cells/ml. For transfection, cortical neurons were pelleted and resuspended to 2×10^6 cells/ml in Internal Neuronal Buffer (INB) (KCl 135 mM, $CaCl_2$ 0.2 mM, $MgCl_2$ 2 mM, HEPES 10 mM, EGTA 5 mM, pH 7.3). 25 µl were placed into wells of a 96-well electroporation plate (BTX Harvard Apparatus 45–0450) and mixed with 25 µl of INB containing 1 µg EGFP plasmid and 4 µg test plasmid. A 350 V, 300 µs pulse was delivered to each well by an ECM square wave pulse generator (Harvard Apparatus ECM-830) attached to a plate handler (BTX Harvard Apparatus HT-

200). 100 µl of Hibernate E was added to each well following electroporation. For cell culture, 10,000 cells/well were placed in 24-well plates (Greiner Bio-One 662,160) pre-coated with 100 µg/ml poly-d-lysine hydrobromide (Sigma P7886) (> 12 h, 37 °C), followed by 10 µg/ml laminin (Sigma L2020) (> 2 h, 37 °C). For inhibitory substrates, 25 µg/ml Chondroitin Sulfate Proteoglycans (Millipore CC117) were added to 10 µg/ml laminin and incubated concurrently with laminin alone treatments. Cells were maintained at 37 °C, 5% CO_2 in Enriched Neurobasal (ENB) media, modified from (Meyer-Franke et al., 1995), consisting of Neurobasal A (Invitrogen 10,888–022), 50X NeuronCult SM1 Neuronal Supplement (Stemcell Technologies 5711), 1 mM sodium pyruvate (Invitrogen 11360-070), 2 mM GlutaMAX (Invitrogen/Gibco 35050-061), 50 U/ml Penicillin–Streptomycin (Invitrogen 15070-063), 5 µM Forskolin (Sigma F6886).

2.3. Sensory cell dissociation, transfection, and culture

Dorsal root ganglia neurons (DRGs) were isolated from freshly euthanized mice and digested with a solution of collagenase (0.5 mg/ml, Invitrogen 17105-041) and dispase (10 mg/ml, Invitrogen 17100) at 37° for 40 min. Cells were brought to single suspension with pipette trituration and then pelleted at 80 G for 5 min. The cell pellet was resuspended in the P3 Primary Cell Nucleofector kit solution (Lonza CC-4461) and approximately 20,000 DRG neurons were transfected with 1 µg of EBFP-2A-H2B-mCherry or HHEX-2A-H2B-mCherry plasmid DNA using the CA-138 program on the 4D-Nucleofector™ System (Lonza). After transfection 80 ul of warm PNGM™ Primary Neuron Growth Medium (Lonza CC-4461) was added to each electroporation well. The entire resulting cell solution was placed into a single well of a 24-well tissue culture plate (Corning). After 72 h, cells were trypsinized, pelleted at 900 G for 3 min, and then resuspended in 200 ul of warm media. The cell suspension was divided between two wells in a 24-well tissue culture dish. 15 h after replating, the cells were fixed and immunostained with a neuronal specific tubulin rabbit polyclonal antibody (1:2000, Sigma T2200) followed by secondary application of Alexa Fluor® 555 dye (Life Technologies A-21430) and Hoechst dye (0.5 µg/ml, Sigma B2261) to enable nuclei detection.

2.4. Cortical cell culture immunohistochemistry

Cultures were fixed in 4% paraformaldehyde (Electron Microscopy Sciences 15710) for 30 min at room temperature, rinsed five times, blocked and permeabilized (PBS, 20% goat serum (Invitrogen 16210-064), 0.2% Triton X-100 (G-Biosciences 786-513) for 30 min at room temperature, and incubated in primary antibody solution (PBS, 10% goat serum, 0.2% Triton X-100, primary antibodies: rabbit anti-βIII-tubulin (1:500, Sigma T2200), mouse anti-Tau-1 (1:1000, Millipore MAB3420), rabbit anti-MAP2 (1:2000, Millipore AB5622), mouse anti-HHEX (1:200, Sigma SAB1403914)) (overnight, 4 °C). After five washes, cultures were incubated in secondary antibody solution containing DAPI nuclear stain (PBS, 10% goat serum, 0.2% Triton X-100, 300 nM DAPI, dilactate (molecular probes D3571) Secondary antibodies: Alexa Flour 647 goat anti-rabbit IgG (1:500, Invitrogen A21245), Alexa Fluor 488 goat anti-mouse IgG (1:500, Invitrogen A11001)) for 2 h at room temperature. Plates were washed five times, and left in 1 ml PBS for imaging.

2.5. Cortical and DRG tissue staining

Adult brains were snap frozen, cryosectioned into 20 μm sections, post-fixed in 4% PFA (20 min, room temperature), blocked (1 h, room temperature), and incubated in primary antibody solution (primary antibodies: anti-HHEX (1:100, Sigma SAB1403914, LSBio LSB3077), anti-NeuN (1:100, MAB377A5)) overnight at 4 °C. After five washes with PBS, sections were incubated in secondary antibody solution (2 h, room temperature), and stained with 300 nM DAPI (20 min, room temperature). Slides were washed with PBS three times and mounted with Fluoro-gel (Electron Microscopy sciences 1798510). CST retrograde labeling was performed on injured animals as in (Wang et al., 2015). Briefly, a 0.85 mm deep lesion was made 1 mm to the left of the midline between C4/C5. 1 μl CTB-Alexafluor 647 (Life Technologies C-34,778) was injected at C4/C5 seven days prior to sacrifice and snap freezing.

2.6. Imaging and quantification of neurite length

For neurite outgrowth assays, Cellomics Cell Insight NXT (Thermo Scientific) acquired images of 3 channels: nuclei (DAPI), neurite staining (βIII-tubulin), and reporter (EGFP), and Cellomics Scan v6.4.0 (Thermo Scientific) traced neurites and quantified reporter intensity. Average total neurite length was quantified for the 10% of cells with greatest EGFP intensity per plate (n > 100 cells per treatment). Average neurite length was normalized to mCherry control for each plate. Each treatment was tested at least three times; those that differed significantly from mCherry control were flagged as hit genes (*p < .05 ANOVA with post-hoc Dunnett's). For axon growth and differentiation assays, a fluorescent inverted microscope was used to identify mCherry + MAP2 + cells as transfected neurons. Axons were identified by Tau-1 staining, and hand traced using NIS-Elements Basic Research software. Axon length for neurons with an axon and percentage of neurons with an axon were quantified for n = 75 cells per treatment. Statistical analysis was paired t-test using Graphpad Prism Software.

For DRG neurite outgrowth assays, a Cellomics ArrayScanXTI (Thermo Scientific) acquired images in 3 channels: nuclei (Hoechst), neurite staining (βIII-tubulin), and reporter (mCherry), and the Neuronal Profiling v4.1 algorithm (Thermo Scientific) traced neurites and quantified reporter intensity. Cells were considered mCherry + when the pixel intensity in the cell reached 2 standard deviations above the mean intensity for mCherry in non-transfected control wells. Average neurite length was normalized to EBFP-2A-H2B-mCherry for each plate. The experiment was repeated three times. Statistical analysis was paired t-test using Graphpad Prism Software.

2.7. Cell survival assay

Cortical neurons were transfected and cultured as previously described, using HHEX as the test gene and an EBFP-2A-mCherry reporter in place of EGFP. After one day in culture, 1 μM staurosporine toxin (Sigma S5921) was added to a subset of EBFP-2A-mCherry wells. The following day media was replaced with either 0.05 μM Calcein AM (Life Technologies C3099), or 0.01 μM Yo-Pro-1-Iodide

(Life Technologies Y3603), both in PBS and containing 1 μg/ml Hoechst 33342 (Molecular Probes H1399), and incubated (30 min, 37 °C). Cellomics Cell Insight NXT (Thermo Scientific) acquired images for three channels: nuclear (Hoechst 33,342), cell survival stain (Calcein AM or Yo-Pro), and reporter (EBFP-2A-mCherry); compartmental analysis quantified intensities for each channel, and data were exported to Excel for analysis. The percentage of surviving cells (Hoechst +/Calcein AM +) and the percentage of apoptotic cells (Hoechst +/Yo-Pro-1-Iodide +) were quantified in five independent experiments. Statistical analysis was by ANOVA with post-hoc Dunnett's was performed using Graphpad Prism Software.

2.8. Western blotting

Lysates for Western blotting were prepared from HEK293 cells that were transfected with either EBFP-2A-H2B-mCherry or HHEX-2A-H2B-mCherry plasmids according to manufacturer's instructions (Lipofectamine 2000, Invitrogen 11668-027). Two days post incubation, cells were lysed using 200 μl lysis buffer (150 Mm sodium chloride, 1.0% Triton-X 100, 0.5% sodium deoxycholate, 0.1% SDS, 50 Mm Tris with protease inhibitors according to manufacturer's instructions (Roche 5892791001)), and cell debris was removed through centrifugation at 4° for 15 min at 21,000 rcf. P3 cortex, adult cortex and adult DRGs tissues were collected into 200-500 μl lysis buffer, and lysed using a homogenizer (VWR KT885450-0020), incubated on ice for 30 min and cell debris was removed through centrifugation at 4°. Protein concentration was estimated using the BCA method. A portion of the lysate (10–40 μg of protein) was fractionated by SDS-polyacrylamide gel electrophoresis (SDS-PAGE), and the separated proteins were transferred to a PVDF membrane. Specific antibodies (Sigma SAB1403914; LSBio LSB3077; 1:1000 dilution) were used to probe for HHEX protein. Immune complexes were detected with suitable secondary antibodies and chemiluminescence reagents (ThermoScientific). β-actin primary antibody (ab6276, 1:2500 dilution) was used to ensure equal gel loading and transfer.

3. Results

3.1. High content screening of cancer related transcription factors

We first used existing datasets to examine the potential overlap between TFs implicated in cancer biology with TFs linked to axon growth. Using the Gene Ranker tool maintained by the Memorial Sloan Kettering Cancer Center, we acquired a list of 1258 genes that are strongly correlated with and/or functionally linked to oncogenesis or tumor suppression. This list contained 254 TFs, as defined by Gene Ontology terms DNA Binding and Regulation of Transcription, DNA Template. Of these, 166 TFs are expressed in the adult and/or developing cortex according to the Allen Brain Atlas (Supplementary Table 1). Intriguingly, these 166 cancer-related TFs included many genes that are already known to regulate axon growth, including 9 out of 10 factors discussed in a recent review of the transcriptional control of axon growth (ATF3, CREB, JUN, KLF4 and -6, NFKB1, SNON, the SOXC family, STAT3, and p53/TP53) (Gao et al., 2004, Qiu et al., 2005, Stegmuller et al., 2006, Gallagher et al., 2007, Seijffers et al., 2007, Jankowski et al., 2009, Moore et al., 2009, Tedeschi et al., 2009, Lerch et al., 2014 and Wang et al., 2015).This high degree of overlap supports the notion of common transcriptional mechanisms that influence growth across diverse cell types, and raised the question of whether other cancer-implicated TFs on the list, many of which are unstudied in a neuronal context, might also act as regulators of axon growth.

We therefore used an established high content screening approach to quantify how cancer-related TFs affected neurite outgrowth when expressed in cortical neurons (Moore et al., 2009, Blackmore et al., 2010 and Lerch et al., 2014). Sixty-nine cancer-related TFs were examined. Importantly, this subset was an effectively random sample based on availability in pre-made expression libraries (Open Biosystems), and not selected by user prioritization. Postnatal rat cortical neurons were co-transfected with plasmid DNA encoding test genes and a fluorescent reporter plasmid and then cultured on laminin substrate. Two days later, automated microscopy (ThermoScientific CellInsight Nxt) quantified neurite outgrowth from

cells identified as neurons through βIII tubulin immunostaining (Fig. 1B) and positive for transfection through expression of EGFP reporter (Fig. 1C). Each gene was tested in three independent experiments, and neurite lengths were normalized to mCherry control (Supplementary Table 1). The set of "cancer" genes included JUN, a known promoter of neurite growth, as well as KLF4 and KLF6, shown previously to inhibit and promote neurite growth, respectively (Moore et al., 2009, Blackmore et al., 2010 and Lerch et al., 2014). These genes therefore functioned as positive controls. As expected, KLF4 significantly reduced (73.3% ± 3.7%, $p < 0.01$) and KLF6 and JUN expression significantly increased (125.8% ± 5.6%, 126.2% ± 6.9%, $p < 0.01$) neurite lengths, confirming the screen's ability to detect TF-evoked changes in neurite length. Notably, in addition to the controls, 6 candidate genes significantly altered neurite lengths, with 2 acting as growth enhancers and 4 as suppressors (Fig. 1E). In summary, nearly 15% of candidate TFs, selected on the basis of their involvement in cellular growth outside the nervous system, displayed an ability to modulate neurite outgrowth in primary neurons.
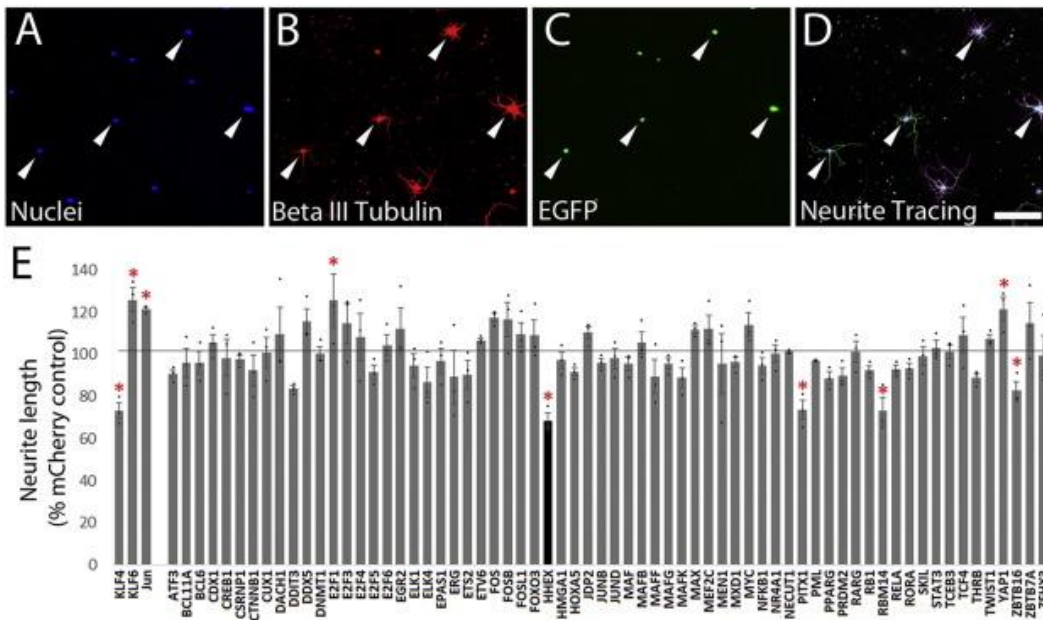

Fig. 1. Phenotypic screening of oncogenic and tumor suppressive transcription factors identifies HHEX as an inhibitor of neurite outgrowth. P3 cortical neurons were co-transfected with EGFP and either mCherry control or test plasmid and cultured on laminin substrates for two days. (A–D) Images were acquired through automated microscopy (nuclear: DAPI, neuronal: βIII-tubulin, transfection: EGFP). Cells positive

for neuron-specific βIII-tubulin and EGFP (arrowheads, B and C) were used for subsequent analyses. (E) Bars show the average neurite length in cells expressing 69 test genes across three replicate experiments (dots), normalized to mCherry control. Test genes included KLF4, KLF6, and JUN, all of which showed expected changes in neurite length, confirming assay sensitivity. Six additional test genes significantly altered neurite length, two positively and four negatively. HHEX (black bar) strongly and consistently inhibits neurite outgrowth. *p < .05 ANOVA with post-hoc Dunnett's, N > 100 cells in three replicate experiments. Scale bar is 50 μm.

3.2. HHEX inhibits axonogenesis without affecting viability

The homeodomain factor HHEX emerged from the initial screening experiment as one of the most potent and consistent inhibitors of neurite outgrowth, and was prioritized for additional analysis. To better characterize the effects of HHEX on neuronal morphology we performed a time-course experiment with axon-specific Tau1 antibodies (Fig. 2). Postnatal cortical neurons were transfected with either HHEX plasmid DNA or EBFP control, and axon formation and length were quantified by hand tracing of Tau1-positive neurites. About 35% of control-transfected neurons extended an axon (Tau1 + process) within 24 h of plating, and the percent of axon-bearing neurons increased steadily to a plateau of about 90% by three days in vitro (DIV; Fig. 2C). In contrast, within 24 h of plating only 21% of HHEX-transfected neurons extended a Tau + axon (Fig. 2C), and the percent of axon-bearing HHEX-transfected neurons never rose above 45%. These data confirm that HHEX expression interferes with axonogenesis.
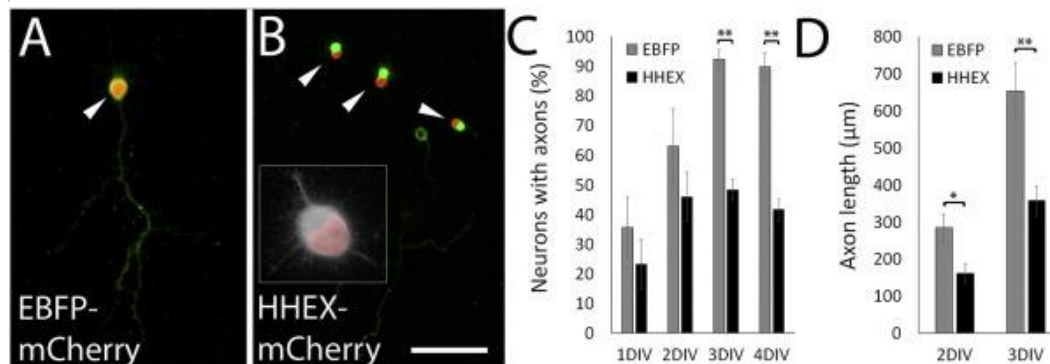

Fig. 2. HHEX expression reduces axon formation and elongation. P3 cortical neurons were transfected with HHEX-2A-mCherry or EBFP-2A-mCherry control and cultured for 1 to 4 days in vitro (DIV). (A,B) Tau1 immunohistochemistry (green) identifies axons in neurons cultured for three days. Transfected neurons are identified by mCherry

fluorescence (arrowheads). Neurons expressing EBFP control extended long axons, whereas neurons transfected with HHEX extended no axons or short axons (arrowheads, B, inset is HHEX phenotype in higher magnification with βIII tubulin in white). (C) Quantification of the percent of neurons with Tau1 + processes shows a significant reduction in axon differentiation in HHEX expressing cells at the 3 and 4 day timepoint. (D) Quantification of axon length, based only on neurons that possessed a Tau1 + process, shows significant reduction in HHEX-expressing neurons compared to control at 2 and 3 days in vitro. * $p < .05$, ** $p < .01$, paired t-test, N > 40 cells each of three replicate experiments. Scale bar is 50 μm.

To determine whether HHEX also affects the rate of extension of existing axons we hand-traced Tau1 + processes at 2 and 3DIV; quantification at 4DIV was prevented by overgrowth of axons that prevented clear discrimination of the cell of origin. At 2DIV, axon length in HHEX-expressing neurons was 44% lower than control (161 μm ± 26.7 μm SEM versus 284.4 μm ± 36.8 μm SEM; $p < 0.01$, paired T-test) (Fig. 2D). Over the next 24 h, control neurons increased average axon lengths to 653.3 μm ± 76.4 μm SEM (an average net addition of 368.9 μm), while HHEX-expressing neurons increased to 357.5 μm ± 40.0 μm SEM, (an average net addition of 195.5 μm). These data indicate that HHEX expression does not simply delay axon formation, but also slow net axon growth between 2DIV and 3DIV. Consistent with this, a time-course analysis using automated tracing showed that HHEX and EBFP-transfected neurons displayed similar neurite lengths at the one day time-point, but that the subsequent daily increases in neurite length were more than 50% lower in HHEX-expressing neurons (Supplemental Fig. 1). Thus HHEX expression also appears to decrease the rate of elongation of extant processes.

We next considered the possibility that the effect of HHEX on axon growth could be secondary to a reduction in cell viability. This issue is particularly important given the involvement of HHEX in cell proliferation in non-neuronal cells, and findings that modulation of cell cycle regulators can induce apoptosis in post-mitotic neurons (Kranenburg et al., 1996 and Nguyen et al., 2002; Greene et al., 2004 and Hoglinger et al., 2007). Cortical neurons were transfected with HHEX or EBFP control plasmid carrying mCherry reporter, and a third group of EBFP-transfected neurons were treated with the toxin staurosporine as a positive control for reduced viability. After two days in culture, a time point at which effects on axon growth are robust (Fig. 2), Cellomics image analysis quantified the percent of transfected (mCherry +) neurons that stained positively for Yo-Pro-1-Iodide or

Calcein AM, indicators of apoptotic and live cells respectively (Fig. 3A–F). As expected, staurosporine elevated Yo-Pro and decreased Calcein signal, confirming the sensitivity of the assay. In contrast, HHEX-transfected neurons showed neither elevated Yo-Pro signal nor decreased Calcein compared to EBFP control (Fig. 3G). Combined, these experiments confirm that HHEX overexpression interferes with axonogenesis and slows axon elongation, without any corresponding decrease in cell viability.
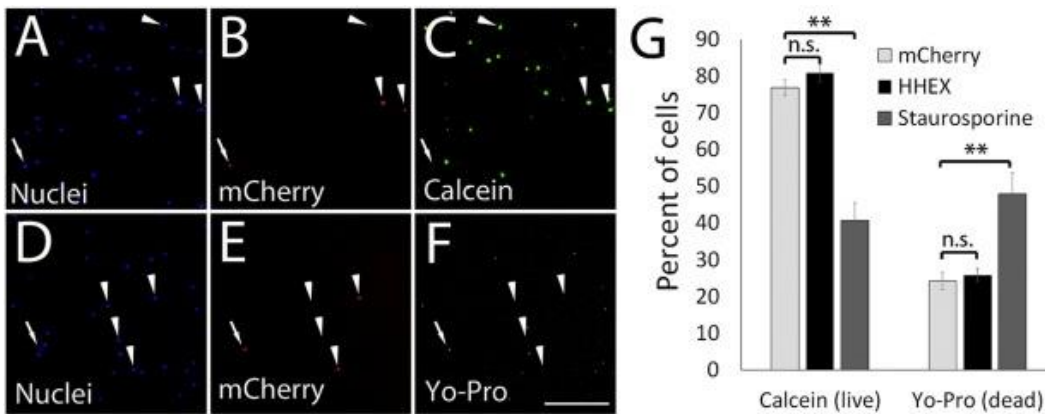

Fig. 3. Cell viability is unaffected by HHEX overexpression. P3–P5 cortical neurons were transfected with HHEX or EBFP control along with mCherry reporter and cultured for two days. Staurosporine toxin was added to a subset of EBFP-transfected cells as a positive control for detection of altered viability. Cells were visualized with DAPI (A,D), mCherry reporter (B,E), and live cell indicator calcein (C) or the dead cell indicator Yo-Pro (F). Arrowheads indicate nuclei (DAPI, A and D) associated with transfected cells (mCherry positive, B and E) that are alive (positive for calcein, C, or negative for Yo-Pro, F). (G) Quantification based on cellomics automated microscopy shows that staurosporine significantly reduces the percent of calcein-positive cells and increases the percent of Yo-Pro positive cells, whereas HHEX expression had no effect. **p < .01, n.s. p > .05, ANOVA with post-hoc Dunnett's. N > 200 transfected cells from each of six replicate experiments. Scale bar is 50 μm.

3.3. Mutation analysis suggests transcriptional repression as relevant mechanism

Wild type HHEX protein is comprised of a DNA binding domain flanked by an N-terminal domain that mediates transcriptional repression (Tanaka et al., 1999), and a C-terminal domain that mediates transcriptional activation (Kasamatsu et al., 2004 and Soufi and Jayaraman, 2008). Thus, depending on cellular context, HHEX can either activate or repress target genes, raising the question of which

activity is relevant to the suppression of axon growth. We therefore created HHEX truncation mutants that lacked either the activation domain (HHEX-ΔC) or the repression domain (HHEX-ΔN), and tested their effects on neurite outgrowth in cortical neurons, as described above (Fig. 4). All constructs included a 2A-H2B-mCherry fluorescent reporter, allowing specific identification of transfected cells. In addition, the fluorescent reporter, as well as direct immunohistochemistry for HHEX protein, confirmed effective expression of all constructs. Removal of the repression domain, but not the activation domain, completely abolished growth inhibition, suggesting that transcriptional repression may be necessary for HHEX's effects on neurite growth (Fig. 4B). Moreover, a chimeric construct in which the endogenous HHEX N-terminal domain was replaced by an alternative Engrailed repression domain phenocopied the full length HHEX repression of neurite outgrowth. This result indicates that transcriptional repression per se, as opposed to a non-transcriptional activity localized to the N-terminal HHEX sequence, causes inhibition of axon growth. Combined, these data identify transcriptional repression domains as both necessary and sufficient for HHEX's inhibition of neurite growth, and suggest a model in which HHEX normally inhibits gene targets that are needed for efficient neurite extension.
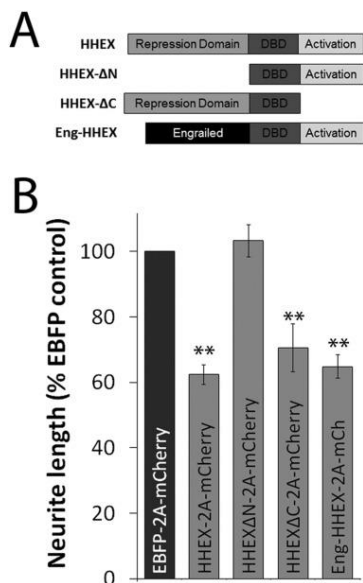

Fig. 4. A transcriptional repression domain is both necessary and sufficient for HHEX's inhibition of neurite growth. Domain-deletion and domain-swapped HHEX mutants, shown schematically in (A), or EBFP control plasmids were overexpressed in early

15

postnatal cortical neurons and cultured for two days. (B) Neurite outgrowth was quantified by automated microscopy. HHEX-ΔC inhibits neurite growth similarly to full length HHEX, showing that the C-terminal activation domain is dispensable for growth inhibition. In contrast, removal of the N-terminal domain abolished growth inhibition. Finally, Engrailed-HHEX also inhibits neurite growth. These experiments suggest that HHEX likely inhibits neurite outgrowth through a mechanism of transcriptional repression. **$p < .01$, ANOVA with post-hoc Dunnett's. N > 150 transfected cells in each of five replicate experiments.

3.4. HHEX is expressed in adult CNS neurons

Although CNS expression is suggested by in situ data from the Allen Brain Atlas, HHEX has been previously described only in hematopoietic lineages and in endoderm-derived tissues such as thyroid, pancreas, liver, and lung (Bogue et al., 2000 and Soufi and Jayaraman, 2008). To establish HHEX's relevance to axon growth it is therefore essential to examine its endogenous pattern of expression in the nervous system. We first validated two anti-HHEX antibodies using HHEX-transfected HEK293 cells. As expected, control-transfected 293 cells displayed no HHEX expression by immunohistochemistry or Western blotting, whereas HHEX-transfected cells showed clear signal with both antibodies (Supplemental Fig. 2). These data demonstrate the specificity of the anti-HHEX antibodies in both immunohistochemistry and Western blotting experiments.

We first examined HHEX expression in the adult murine cortex by Western blot, and observed a clear ~ 42 kD band at the same position as overexpressed full-length HHEX (Fig. 5A). These data confirm expression of HHEX protein in the adult cortex. In contrast, cortex from postnatal day 3 (P3), the age at which cells were prepared for neurite outgrowth assays, did not show detectable expression of HHEX by Western blotting. Consistent with this, immunohistochemistry on cultured P3 cortical neurons detected no endogenous HHEX in cells transfected with EBFP control plasmid, but did confirm the presence of HHEX protein in cells transfected with HHEX plasmid (Fig. 5B–E). Combined, these data demonstrate expression of HHEX in cortical tissue of adult but not early postnatal age.
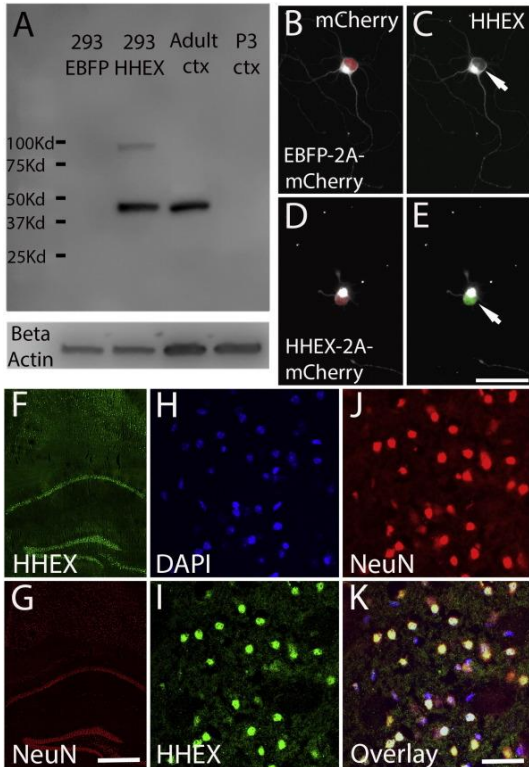
Fig. 5. HHEX is widely expressed in adult, but not neonatal, CNS neurons. (A) Western blotting detects HHEX in 293 cells transfected with HHEX plasmid, but not in EBFP-transfected control cells, confirming antibody specificity. HHEX protein is also detected in adult murine cortex, but not in postnatal tissue at the age used to prepare neurons for cell culture. (B–E) P3 cortical neurons were transfected with EBFP-2A-H2B-mCherry control plasmid or HHEX-2A-H2B-mCherry and cultured for two days. mCherry expression (red, B,D) identifies transfected cells, and immunohistochemistry for βIII tubulin (white) identifies neurons. Immunohistochemistry detects HHEX in HHEX-transfected neurons (green, arrow, E), but not in control transfected neurons (arrow, C). Adult hippocampus (F,G) or cortex (H–K) was stained with DAPI (nuclei, H), anti-NeuN antibody (J,G) and anti-HHEX antibody (F,I). In both brain regions, endogenous HHEX expression co-localized with NeuN confirming widespread expression of HHEX in neuronal nuclei in the CNS. Scale bars are 50 μm (E), 500 μm (G), and 20 μm (K).

To further explore the relationship between HHEX protein expression and neurite length we visualized HHEX protein in HHEX-transfected or EBFP-transfected control neurons while simultaneously measuring neurite lengths. Quantification of the intensity of HHEX immunohistochemistry signal in HHEX-transfected neurons showed a range of intensities above the background level in control cells, indicating variable levels of HHEX protein expression (Supplemental Fig. 3). Analysis of average neurite lengths, binned according to increasing levels of HHEX protein, confirmed a significant reduction in neurite length in neurons with elevated HHEX expression. Neurite

lengths were significantly reduced in neurons with relatively modest HHEX expression, such that neurons within the second quintile of HHEX intensity were 71.2% of control length (p < .05, ANOVA with Dunnet's post-hoc), with neurons in the brightest HHEX quintile averaging 56.1% of control. These data confirm with direct detection that increased expression of HHEX protein in postnatal cortical neurons reduces neurite outgrowth.

To determine whether HHEX is expressed specifically in neurons in the adult brain, as opposed to other cell types, we examined murine brain sections by immunohistochemistry, using NeuN as a neuronal marker. Intriguingly, we observed a striking and complete overlap between HHEX and NeuN reactivity (Fig. 5F–K). HHEX was detected in all NeuN + nuclei examined in the forebrain, midbrain and hindbrain and was not detected in adjacent NeuN-negative nuclei, indicating expression that is widespread and highly specific to neurons. To confirm these findings we repeated the experiment with a second antibody against HHEX that was raised against a distinct epitope, with identical results (Supplemental Fig. 4). To assess HHEX expression in CNS neurons that are responding to axotomy, we performed spinal transections and injected retrograde tracers to the injury site to identify axotomized corticospinal tract (CST) neurons. Two weeks post-injury, HHEX was readily detectable in all injured CST neurons, and the intensity of staining appeared neither elevated nor decreased (Fig. 6). These data show expression of HHEX protein in the adult CNS neurons, including CST neurons after spinal injury.
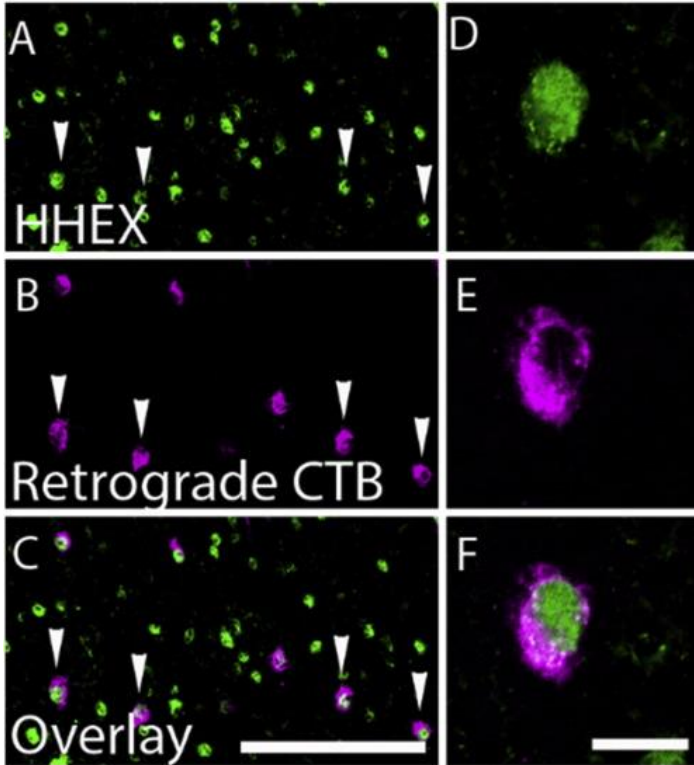
Fig. 6. HHEX is expressed in corticospinal tract (CST) neurons after axotomy. CST axons were severed in the cervical spinal cord of adult mice and the retrograde tracer cholera toxin B (CTB) conjugated to Alexafluor 647 (CTB-647) injected to the injury site. Two weeks later cortical sections were prepared and immunohistochemistry for HHEX performed. A and D show HHEX expression, B and E show retrogradely identified CST neurons, and C and F show the overlap. Arrows indicate CST neurons with clear HHEX signal. Scale bars are 100 μm (C) and 10 μm (F).

Axon growth in the adult CNS is constrained in part by inhibitory substrates such as chondroitin sulfate proteoglycans (CSPGs) (Carulli et al., 2005). We therefore explored potential interactions between CSPG substrates and HHEX expression by culturing neurons on substrates of laminin (10 μg/ml) or a mixture of laminin and CSPGs (10 μg/ml laminin, 25 μg/ml CSPGs) and performing immunohistochemistry for HHEX. HHEX was detectable on neither substrate, and automated microscopy confirmed similar levels of HHEX signal on laminin and CSPG substrates. As a positive control the immunohistochemistry, HHEX was readily detectable in HHEX-transfected cells. (Fig. 7A–E). These data indicate that HHEX expression is insensitive to CSPG exposure.
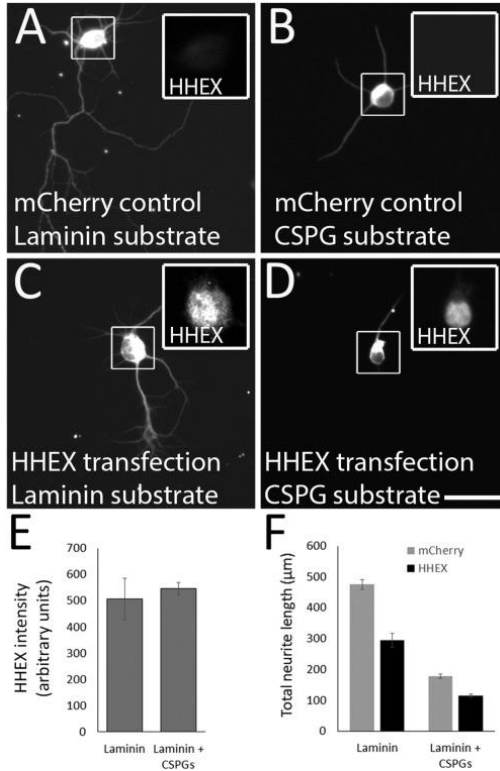
Fig. 7. HHEX inhibits neurite outgrowth independently of chondroitin sulfate proteoglycan signaling. Cortical neurons were transfected with EBFP control plasmid or HHEX and cultured for three days on laminin or a laminin/CSPG mixture. Automated image analysis quantified the intensity of HHEX immunohistochemistry and the length of neurites. (A–D) HHEX protein was not detected EBFP-transfected neurons on laminin (inset, A) or CSPG (inset, B) substrate, but was readily visible in HHEX-transfected neurons (insets, C,D). (E) Quantification of HHEX immunohistochemistry performed on untransfected neurons shows no significant change in HHEX expression as a result of exposure to CSPG substrates (p > .05, paired t-test, N > 2000 neurons). (F) Neurite lengths were significantly reduced on CSPG substrates. On both laminin and CSPG substrates, transfection with HHEX plasmids decreased neurite lengths compared to EBFP control. **p < .01, two way ANOVA, N > 100. Scale bar is 10 μm.

Next, to test whether HHEX-mediated inhibition of neurite outgrowth was affected by CSPG substrates, neurons were transfected with HHEX or control plasmid and cultured on laminin or CSPG substrates. As expected, neurite outgrowth by control-transfected neurons was reduced on CSPG substrates (69.9% shorter than on laminin) (Fig. 7F). On laminin substrate, HHEX expression caused a 39% reduction in neurite length compared to mCherry control. On CSPG substrates, HHEX also reduced neurite lengths, and did so to a degree that was proportional to the effect on laminin (35% shorter than control-transfected neurons on CSPGs). Combined with the insensitivity of HHEX expression to CSPG, these data suggest that the

20

molecular mechanisms that mediate growth inhibition by HHEX function independently of those triggered by CSPG substrates.

3.5. HHEX expression and function in peripheral neurons

We next examined HHEX expression in peripheral neurons of the dorsal root ganglia (DRG), which possess a generally higher regenerative capacity than CNS neurons. Immunohistochemistry for HHEX showed very dim signal in sections of adult DRG; as a positive control, adult cortical tissue processed in parallel and visualized with identical acquisition parameters showed bright HHEX signal (Fig. 8A, B). Similarly, Western blotting in DRG tissue detected very faint size-shifted bands, but no HHEX protein in a position corresponding to overexpressed HHEX protein or to protein detected in adult cortex (Fig. 8C). Adult DRG neurons are known to extend lengthy processes when placed in culture, and this response requires extensive transcriptional changes that occur in the days after plating. We therefore performed immunohistochemistry for HHEX in DRG neurons that were transfected with EBFP-2A-H2B-mCherry control or HHEX-2A-H2B-mCherry and maintained in culture for three days (Fig. 8D–G). HHEX protein was not detected in control-transfected DRG neurons, but was readily detectable in HHEX-transfected cells (Fig. 8D–G). Combined, these data suggest that unlike CNS neurons, regeneration-competent PNS neurons do not express detectable amounts of HHEX protein in neither the uninjured state, nor when engaged in injury-triggered axon growth.
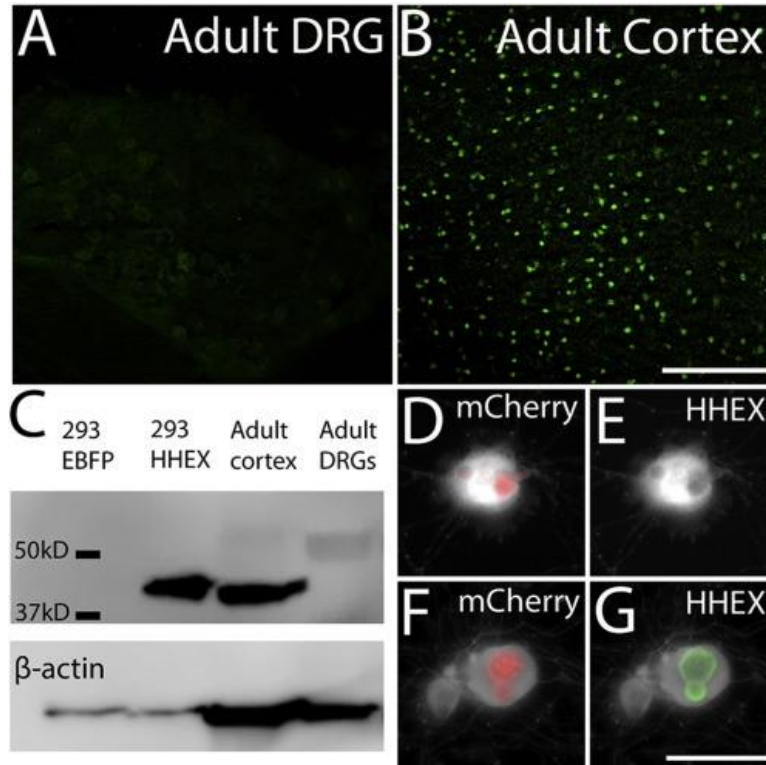
Fig. 8. HHEX is more abundant in the central than in the peripheral nervous system. (A,B) Dorsal root ganglia (DRG, A) and cortex (B) were stained in parallel with anti-HHEX antibodies. HHEX is readily detectable in cortex but, using identical acquisition parameters, was not detected in DRG tissue. (C) Western blotting detects HHEX protein in HHEX-transfected 293 cells and adult cortex, but detects only faint and size-shifted protein bands in DRG tissue. (D–G) Adult DRG neurons were transfected with control EBFP-2A-H2B-mCherry (D,E) or HHEX-2A-H2B-mCherry (F,G), cultured on laminin substrate for four days, followed by immunohistochemistry for βIII tubulin (white) and HHEX (green, E,G). HHEX was not detected in EBFP-transfected DRG neurons, but was readily detected in HHEX-transfected cells. Scale bars are 100 μm (A) and 50 μm (D–G).

We therefore tested the effects of elevating full-length HHEX expression in DRG neurons. Cultured DRG neurons were transfected with plasmids encoding HHEX or EBFP, maintained for the three days, and then replated to remove existing neurites. The amount of neurite growth generated in the subsequent 24 h was then quantified. This paradigm avoids technical problems associated with excessive axon growth by DRG neurons during the lag between plasmid transfection and protein function. Immunohistochemistry confirmed exogenous HHEX expression (Fig. 8F, G). Compared to EBFP control, HHEX expression significantly reduced the number of neurites by 2-fold and the total length of neurites produced by DRG neurons (Fig. 9). Combined, these data demonstrate that ectopic expression of full-

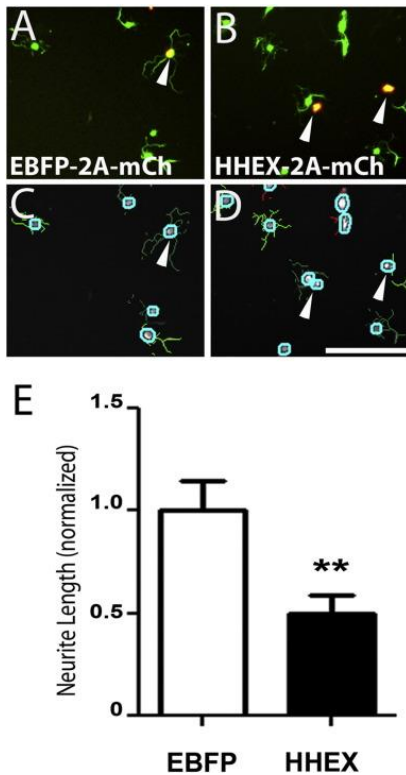length HHEX, normally absent in PNS neurons, is sufficient to reduce the regenerative capacity of DRG neurons.

Fig. 9. HHEX overexpression reduces DRG neurite outgrowth. Adult DRG neurons were transfected with EBFP-2A-H2B-mCherry (A,C) or HHEX-2A-H2B-mCherry (B,D), maintained for three days, re-plated to remove existing neurites, and then maintained for one additional day. Neuron-specific tubulin (green, A,B) identifies neurites and mCherry (arrowheads, A,B) identifies transfected cells. (C,D) Neurite outgrowth was quantified with the Neuronal Profiling Algorithm on a Cellomics ArrayScanXTI High Content Analysis microscope (ThermoFisher) after imaging and mask creation. Cell bodies are indicated by blue circles, and neurites are shown in green or red. (E) Neurite outgrowth was normalized to the average total neurite length for EBFP-2A-H2B-mCherry transfected DRGs. N > 100 cells in three replicate experiments, **p < 0.001, paired t-test. Scale bar is 150 μm.

4. Discussion

This study used a screening approach to identify the homeodomain factor HHEX, previously studied as a tumor suppressor in hematopoietic and endodermal lineages, as a potent suppressor of axon growth when overexpressed in CNS neurons. Our data suggest that HHEX may act through a mechanism of transcriptional repression to reduce both axon initiation and extension, without negatively affecting cell viability. Moreover, HHEX is endogenously expressed in

the nuclei of CNS neurons, including CST neurons after axotomy. In contrast, peripheral DRG neurons express much lower levels of HHEX, and forced expression of HHEX reduces DRG axon growth. Combined, the phenotypic effects and pattern of expression support the hypothesis that transcriptional repression by HHEX may limit axon growth in CNS neurons.

4.1. Transcriptional inhibition of axon growth

In contrast to HHEX, the majority of TFs that have previously been linked to axon growth appear to play pro-regenerative roles, likely by coordinating the production of multiple growth-associated proteins. Prominent examples include JUN, ATF3, KLF7, SOX11, STAT3, and CREB, all of which are active in neurons that mount successful axon regeneration but are missing or inactive in non-regenerating cell types (Gao et al., 2004 and Qiu et al., 2005; Seijffers et al., 2007, Jankowski et al., 2009, Blackmore et al., 2012 and Lerch et al., 2014). Accordingly, we and the others have pursued forced expression of these TFs as a strategy to enhance axon growth (Qiu et al., 2005, Seijffers et al., 2007, Jankowski et al., 2009, Blackmore et al., 2012, Lerch et al., 2014 and Wang et al., 2015). It is well appreciated, however, that regenerative ability can also be held in check by the presence of cell-intrinsic factors that limit growth potential. Thus, at the level of gene transcription, it may be necessary to complement the overexpression approach by neutralizing TFs that repress transcription by occupying pro-regenerative loci. The identity of such growth-inhibitory TFs, however, remains unclear. Members of the KLF family, notably KLF4, are likely candidates because they are expressed in poorly-regenerating CNS neurons and contribute to their low regenerative capacity (Moore et al., 2009). Whether KLF4 acts as a transcriptional repressor of pro-regenerative genes, as opposed to alternative mechanisms such as activation of growth inhibitory genes, has not been established.

In this context it is significant that the functional domain analyses suggest that HHEX inhibits axon growth through a mechanism of transcriptional repression. Although HHEX is known to be capable of either activating or repressing target genes, the domain deletion experiments showed that a known activation domain is

dispensable, and a known repression domain essential, for inhibition of neurite outgrowth. In addition, evidence that the Engrailed repression domain can effectively substitute for the endogenous HHEX repression domain makes it likely that transcriptional repression, and not an alternative function specific to the HHEX N-terminal sequence, drives inhibition of neurite growth. Direct assays of transcriptional activity (e.g. luciferase assays with promoter mutations/deletion) are needed to confirm HHEX's transcriptional mode of activity, but the experiments reported here support a working model in which HHEX transcriptionally represses gene products needed for efficient axon growth.

HHEX is relatively unstudied in the nervous system, but well characterized in other systems. HHEX functions as an essential regulator of vertebrate development, controlling hematopoietic and vascular system formation as well as formation of the vertebrate body axis early in development (Soufi and Jayaraman, 2008). HHEX is also essential for the formation and maintenance of organs derived from the foregut endoderm such as thyroid, liver and lung (Bogue et al., 2000). HHEX knockout animals die embryonically around day 12 and show anterior truncation including a lack of forebrain tissue, but this defect has been interpreted as secondary to defects in the anterior visceral endoderm signaling center (Martinez-Barbera et al., 2000 and Martinez Barbera et al., 2000).

In adult mammals, we find that full length HHEX is widely expressed in neurons throughout the central nervous system, with expression localized to neuronal nuclei. Consistent with a role for HHEX in axon growth inhibition, we observe that CST neurons, which are generally refractory to regenerative axon growth, display HHEX expression after spinal injury. In contrast, HHEX appears to be much less abundant in early postnatal cortical neurons and in DRG neurons, both constitutively and during injury-triggered axon growth. When full length HHEX is overexpressed in early postnatal cortical neurons or DRG neurons, both of which are innately regeneration competent, we observe defects in both axon formation and extension. Immunohistochemistry showed that significant reductions in neurite length occurred in neurons with relatively dim immunohistochemistry HHEX signal. Although comparison between immunohistochemistry experiments must be made cautiously, it is notable that the intensity

of HHEX signal that produced significant reductions in neurite length in cultured neurons appeared comparable to or dimmer than the intensity of endogenous HHEX in the adult brain. Combined, these data are consistent with the notion that endogenous HHEX expression in adult neurons may restrict axon growth.

The identity of HHEX target genes in neurons remains unclear. In various proliferative cell types, a number of genes have been shown to change in expression upon HHEX overexpression or knockdown, including ESM1, VEGF, SST, KIT, and cyclin dependent kinases and associated inhibitors (Noy et al., 2010, Shields et al., 2014, Zhang et al., 2014 and Jackson et al., 2015). In the case of ESM1, VEGFR, and SST direct binding of HHEX to promoter sites has been demonstrated, whereas other gene targets may be direct or indirect (Cong et al., 2006, Noy et al., 2010 and Zhang et al., 2014). In either case, the link between these known targets and the suppression of axon growth is not obvious. Intriguingly, HHEX has also been shown to inhibit the activity of JUN, a well-studied transcriptional promoter of axon growth that we confirmed here to increase neurite length (Schaefer et al., 2001, Raivich et al., 2004 and Lerch et al., 2014). HHEX was also recently shown to negatively regulate the activity of MYC, a TF implicated in cellular growth and proliferation, and very recently linked to axon regeneration in the optic system (Belin et al., 2015 and Marfil et al., 2015). Determining direct and indirect gene targets of HHEX in neurons, and clarifying the potential interactions of HHEX with JUN and/or MYC in the context of axon growth, represents important directions for future research.

4.2. Oncogenes and tumor suppressors as regulators of axon growth

The general notion that intracellular factors implicated in cancer biology could regulate axon growth has been previously proposed (Park et al., 2008). Axon growth may depend on catabolic processes and cytoskeletal dynamics that contribute to cell proliferation and motility, much like what is observed in cancerous cells. Conversely, tumor suppressive molecules are in place to prevent aberrant growth upon maturation. Since many of these genes are expressed in post-mitotic neurons, it raises a possibility that the tumor suppressor genes

may inhibit axonal growth and contribute to the reduced regenerative capacity observed in mature CNS neurons. In line with this, the proto-oncogene JUN drives regenerative axon growth (Raivich et al., 2004 and Lerch et al., 2014) whereas the tumor suppressor KLF4 restricts axon growth (Moore et al., 2009).

We therefore undertook a systematic evaluation of this idea by selecting factors based on their tumor suppressor/oncogenic properties and examining their effects on neurite growth. Approximately 13% about 2% (8/428) in a previous screen using similar techniques but which focused on genes that are developmentally regulated (Blackmore et al., 2010). This relatively high hit rate corroborates the concept that mechanisms driving cellular growth and motility are conserved across cell types. Intriguingly, the two TFs that emerged as growth promoting in the screen (E2F1 and YAP1) are generally considered oncogenic (Alonso et al., 2008 and Liu et al., 2010a), whereas the four growth-suppressors (HHEX, PITX1, RBM14, and ZBTB16) have been described as tumor suppressive (Kolfschoten et al., 2005, Kang et al., 2008, Soufi and Jayaraman, 2008 and Suliman et al., 2012). Although it should be noted that factors cannot always be cleanly classified due to conflicting findings in different cell types (George et al., 2003), the screen results support an overall correlation between oncogenesis and axon growth and tumor suppression with growth inhibition. Thus further study of factors implicated in cancer biology may be a productive means to identify new regulators of axon growth.

Acknowledgments

References

Alonso et al., 2008. M.M. Alonso, R. Alemany, J. Fueyo, C. Gomez-Manzano. E2F1 in gliomas: a paradigm of oncogene addiction. *Cancer Lett.,* 263 (2008), pp. 157–163

Belin et al., 2015. S. Belin, H. Nawabi, C. Wang, S. Tang, A. Latremoliere, P. Warren, H. Schorle, C. Uncu, C.J. Woolf, Z. He, J.A. Steen. Injury-

induced decline of intrinsic regenerative ability revealed by quantitative proteomics, *Neuron,* 86 (2015), pp. 1000–1014

Blackmore and Letourneau, 2006. M. Blackmore, P.C. Letourneau. Changes within maturing neurons limit axonal regeneration in the developing spinal cord*. J. Neurobiol.,* 66 (2006), pp. 348–360

Blackmore et al., 2010. M.G. Blackmore, D.L. Moore, R.P. Smith, J.L. Goldberg, J.L. Bixby, V.P. Lemmon. High content screening of cortical neurons identifies novel regulators of axon growth. *Mol. Cell. Neurosci.,* 44 (2010), pp. 43–54

Blackmore et al., 2012. M.G. Blackmore, Z. Wang, J.K. Lerch, D. Motti, Y.P. Zhang, C.B. Shields, J.K. Lee, J.L. Goldberg, V.P. Lemmon, J.L. Bixby. Kruppel-like factor 7 engineered for transcriptional activation promotes axon regeneration in the adult corticospinal tract. *Proc. Natl. Acad. Sci. U. S. A.,* 109 (2012), pp. 7517–7522

Bogue et al., 2000. C.W. Bogue, G.R. Ganea, E. Sturm, R. Ianucci, H.C. Jacobs. Hex expression suggests a role in the development and function of organs derived from foregut endoderm. *Dev. Dyn.,* 219 (2000), pp. 84–89

Buchser et al., 2010. W.J. Buchser, T.I. Slepak, O. Gutierrez-Arenas, J.L. Bixby, V.P. Lemmon. Kinase/phosphatase overexpression reveals pathways regulating hippocampal neuron morphology. *Mol. Syst. Biol.,* 6 (2010), p. 391

Carulli et al., 2005. Carulli, T. Laabs, H.M. Geller, J.W. Fawcett. Chondroitin sulfate proteoglycans in neural development and regeneration. *Curr. Opin. Neurobiol.,* 15 (2005), pp. 116–120

Case and Tessier-Lavigne, 2005. L.C. Case, M. Tessier-Lavigne. Regeneration of the adult central nervous system. *Curr. Biol.,* 15 (2005), pp. R749–R753

Cong et al., 2006. R. Cong, X. Jiang, C.M. Wilson, M.P. Hunter, H. Vasavada, C.W. Bogue. Hhex is a direct repressor of endothelial cell-specific molecule 1 (ESM-1). *Biochem. Biophys. Res. Commun.,* 346 (2006), pp. 535–545

Gallagher et al., 2007. D. Gallagher, H. Gutierrez, N. Gavalda, G. O'Keeffe, R. Hay, A.M. Davies. Nuclear factor-kappaB activation via tyrosine phosphorylation of inhibitor kappaB-alpha is crucial for ciliary neurotrophic factor-promoted neurite growth from developing neurons. *J. Neurosci.,* 27 (2007), pp. 9664–9669

Gao et al., 2004. Y. Gao, K. Deng, J. Hou, J.B. Bryson, A. Barco, E. Nikulina, T. Spencer, W. Mellado, E.R. Kandel, M.T. Filbin. Activated CREB is sufficient to overcome inhibitors in myelin and promote spinal axon regeneration in vivo. *Neuron,* 44 (2004), pp. 609–621

George et al., 2003. A. George, H.C. Morse 3rd, M.J. Justice. The homeobox gene hex induces T-cell-derived lymphomas when overexpressed in hematopoietic precursor cells. *Oncogene,* 22 (2003), pp. 6764–6773

Gerhard et al., 2004 D.S. Gerhard, *et al.* The status, quality, and expansion of the NIH full-length cDNA project: the mammalian gene collection (MGC). *Genome Res.,* 14 (2004), pp. 2121–2127

Goldberg et al., 2002. J.L. Goldberg, M.P. Klassen, Y. Hua, B.A. Barres. Amacrine-signaled loss of intrinsic axon growth ability by retinal ganglion cells. *Science,* 296 (2002), pp. 1860–1864

Greene et al., 2004. L.A. Greene, S.C. Biswas, D.X. Liu. Cell cycle molecules and vertebrate neuron death: E2F at the hub. *Cell Death Differ.,* 11 (2004), pp. 49–60

Hoglinger et al., 2007. G.U. Hoglinger, J.J. Breunig, C. Depboylu, C. Rouaux, P.P. Michel, D. Alvarez-Fischer, A.L. Boutillier, J. Degregori, W.H. Oertel, P. Rakic, E.C. Hirsch, S. Hunot. The pRb/E2F cell-cycle pathway mediates cell death in Parkinson's disease. *Proc. Natl. Acad. Sci. U. S. A.,* 104 (2007), pp. 3585–3590

Jackson et al., 2015. J.T. Jackson, C. Nasa, W. Shi, N.D. Huntington, C.W. Bogue, W.S. Alexander, M.P. McCormack. A crucial role for the homeodomain transcription factor Hhex in lymphopoiesis. *Blood,* 125 (2015), pp. 803–814

Jankowski et al., 2009. M.P. Jankowski, S.L. McIlwrath, X. Jing, P.K. Cornuet, K.M. Salerno, H.R. Koerber, K.M. Albers. Sox11 transcription factor modulates peripheral nerve regeneration in adult mice. *Brain Res.,* 1256 (2009), pp. 43–54

Kang et al., 2008. Y.K. Kang, R. Schiff, L. Ko, T. Wang, S.Y. Tsai, M.J. Tsai, B.W. O'Malley. Dual roles for coactivator activator and its counterbalancing isoform coactivator modulator in human kidney cell tumorigenesis. *Cancer Res., 68* (2008), pp. 7887–7896

Kasamatsu et al., 2004. S. Kasamatsu, A. Sato, T. Yamamoto, V.W. Keng, H. Yoshida, Y. Yamazaki, M. Shimoda, J. Miyazaki, T. Noguchi. Identification of the transactivating region of the homeodomain protein, hex. *J. Biochem.,* 135 (2004), pp. 217–223

Kita-Matsuo et al., 2009. H. Kita-Matsuo, M. Barcova, N. Prigozhina, N. Salomonis, K. Wei, J.G. Jacot, B. Nelson, S. Spiering, R. Haverslag, C. Kim, M. Talantova, R. Bajpai, D. Calzolari, A. Terskikh, A.D. McCulloch, J.H. Price, B.R. Conklin, H.S. Chen, M. Mercola. Lentiviral vectors and protocols for creation of stable hESC lines for fluorescent tracking and drug resistance selection of cardiomyocytes. *PLoS One,* 4 (2009), Article e5046

Kolfschoten et al., 2005. I.G. Kolfschoten, B. van Leeuwen, K. Berns, J. Mullenders, R.L. Beijersbergen, R. Bernards, P.M. Voorhoeve, R.

Agami. A genetic screen identifies PITX1 as a suppressor of RAS activity and tumorigenicity. *Cell,* 121 (2005), pp. 849–858

Kranenburg et al., 1996. O. Kranenburg, A.J. van der Eb, A. Zantema. Cyclin D1 is an essential mediator of apoptotic neuronal cell death. *EMBO J.,* 15 (1996), pp. 46–54

Lerch et al., 2014. J.K. Lerch, Y.R. Martinez-Ondaro, J.L. Bixby, V.P. Lemmon. cJun promotes CNS axon growth. *Mol. Cell. Neurosci.,* 59 (2014), pp. 97–105

Liu et al., 2010a. A.M. Liu, M.Z. Xu, J. Chen, R.T. Poon, J.M. Luk. Targeting YAP and hippo signaling pathway in liver cancer. *Expert. Opin. Ther. Targets,* 14 (2010), pp. 855–868

Liu et al., 2010b. K. Liu, Y. Lu, J.K. Lee, R. Samara, R. Willenberg, I. Sears-Kraxberger, A. Tedeschi, K.K. Park, D. Jin, B. Cai, B. Xu, L. Connolly, O. Steward, B. Zheng, Z. He. PTEN deletion enhances the regenerative ability of adult corticospinal neurons. *Nat. Neurosci.,* 13 (2010), pp. 1075–1081

Marfil et al., 2015. V. Marfil, M. Blazquez, F. Serrano, J.V. Castell, R. Bort. Growth-promoting and tumourigenic activity of c-Myc is suppressed by Hhex. *Oncogene,* 34 (2015), pp. 3011–3022

Martinez Barbera et al., 2000. J.P. Martinez Barbera, M. Clements, P. Thomas, T. Rodriguez, D. Meloy, D. Kioussis, R.S. Beddington. The homeobox gene Hex is required in definitive endodermal tissues for normal forebrain, liver and thyroid formation. *Development,* 127 (2000), pp. 2433–2445

Martinez-Barbera et al., 2000. J.P. Martinez-Barbera, T.A. Rodriguez, R.S. Beddington. The homeobox gene Hesx1 is required in the anterior neural ectoderm for normal forebrain formation. *Dev. Biol.,* 223 (2000), pp. 422–430

Meyer-Franke et al., 1995. A. Meyer-Franke, M.R. Kaplan, F.W. Pfrieger, B.A. Barres. Characterization of the signaling interactions that promote the survival and growth of developing retinal ganglion cells in culture. *Neuron,* 15 (1995), pp. 805–819

Moore and Goldberg, 2011. D.L. Moore, J.L. Goldberg. Multiple transcription factor families regulate axon growth and regeneration. *Dev. Neurobiol.,* 71 (2011), pp. 1186–1211

Moore et al., 2009. D.L. Moore, M.G. Blackmore, Y. Hu, K.H. Kaestner, J.L. Bixby, V.P. Lemmon, J.L. Goldberg. KLF family members regulate intrinsic axon regeneration ability. *Science,* 326 (2009), pp. 298–301

Nguyen et al., 2002. M.D. Nguyen, W.E. Mushynski, J.P. Julien. Cycling at the interface between neurodevelopment and neurodegeneration. *Cell Death Differ.,* 9 (2002), pp. 1294–1306

Noy et al., 2010. P. Noy, H. Williams, A. Sawasdichai, K. Gaston, P.S. Jayaraman. PRH/Hhex controls cell survival through coordinate

transcriptional regulation of vascular endothelial growth factor signaling. *Mol. Cell. Biol.,* 30 (2010), pp. 2120–2134

Park et al., 2008. K.K. Park, K. Liu, Y. Hu, P.D. Smith, C. Wang, B. Cai, B. Xu, L. Connolly, I. Kramvis, M. Sahin, Z. He. Promoting axon regeneration in the adult CNS by modulation of the PTEN/mTOR pathway. *Science,* 322 (2008), pp. 963–966

Patodia and Raivich, 2012. S. Patodia, G. Raivich. Downstream effector molecules in successful peripheral nerve regeneration. *Cell Tissue Res.,* 349 (2012), pp. 15–26

Pomerantz and Blau, 2013. J.H. Pomerantz, H.M. Blau. Tumor suppressors: enhancers or suppressors of regeneration? *Development,* 140 (2013), pp. 2502–2512

Qiu et al., 2005. J. Qiu, W.B. Cafferty, S.B. McMahon, S.W. Thompson. Conditioning injury-induced spinal axon regeneration requires signal transducer and activator of transcription 3 activation. *J. Neurosci.,* 25 (2005), pp. 1645–1653

Raivich et al., 2004. G. Raivich, M. Bohatschek, C. Da Costa, O. Iwata, M. Galiano, M. Hristova, A.S. Nateri, M. Makwana, L. Riera-Sans, D.P. Wolfer, H.P. Lipp, A. Aguzzi, E.F. Wagner, A. Behrens. The AP-1 transcription factor c-Jun is required for efficient axonal regeneration. *Neuron,* 43 (2004), pp. 57–67

Schaefer et al., 2001. L.K. Schaefer, S. Wang, T.S. Schaefer. Functional interaction of Jun and homeodomain proteins. *J. Biol. Chem.,* 276 (2001), pp. 43074–43082

Seijffers et al., 2007. R. Seijffers, C.D. Mills, C.J. Woolf. ATF3 increases the intrinsic growth state of DRG neurons to enhance peripheral nerve regeneration. *J. Neurosci.,* 27 (2007), pp. 7911–7920

Shields et al., 2014. B.J. Shields, R. Alserihi, C. Nasa, C. Bogue, W.S. Alexander, M.P. McCormack. Hhex regulates Kit to promote radioresistance of self-renewing thymocytes in Lmo2-transgenic mice. *Leukemia* (2014)

Soufi and Jayaraman, 2008. A. Soufi, P.S. Jayaraman. PRH/Hex: an oligomeric transcription factor and multifunctional regulator of cell fate. *Biochem. J.,* 412 (2008), pp. 399–413

Stegmuller et al., 2006. J. Stegmuller, Y. Konishi, M.A. Huynh, Z. Yuan, S. Dibacco, A. Bonni. Cell-intrinsic regulation of axonal morphogenesis by the Cdh1-APC target SnoN. *Neuron,* 50 (2006), pp. 389–400

Suliman et al., 2012. B.A. Suliman, D. Xu, B.R. Williams. The promyelocytic leukemia zinc finger protein: two decades of molecular oncology. *Front. Oncol.,* 2 (2012), p. 74

Sun and He, 2010. F. Sun, Z. He. Neuronal intrinsic barriers for axon regeneration in the adult CNS. *Curr. Opin. Neurobiol.,* 20 (2010), pp. 510–518

Sun et al., 2011. F. Sun, K.K. Park, S. Belin, D. Wang, T. Lu, G. Chen, K. Zhang, C. Yeung, G. Feng, B.A. Yankner, Z. He. Sustained axon regeneration induced by co-deletion of PTEN and SOCS3. *Nature,* 480 (2011), pp. 372–375

Tanaka et al., 1999. T. Tanaka, T. Inazu, K. Yamada, Z. Myint, V.W. Keng, Y. Inoue, N. Taniguchi, T. Noguchi. cDNA cloning and expression of rat homeobox gene, Hex, and functional characterization of the protein. *Biochem. J.,* 339 (Pt 1) (1999), pp. 111–117

Tedeschi et al., 2009. A. Tedeschi, T. Nguyen, R. Puttagunta, P. Gaub, S. Di Giovanni. A p53-CBP/p300 transcription module is required for GAP-43 expression, axon outgrowth, and regeneration. *Cell Death Differ.,* 16 (2009), pp. 543–554

Wang et al., 2015. Z. Wang, A. Reynolds, A. Kirry, C. Nienhaus, M.G. Blackmore. Overexpression of Sox11 promotes corticospinal tract regeneration after spinal injury while interfering with functional recovery. *J. Neurosci.,* 35 (2015), pp. 3139–3145

Yiu and He, 2006. G. Yiu, Z. He. Glial inhibition of CNS axon regeneration. *Nat. Rev. Neurosci.,* 7 (2006), pp. 617–627

Zhang et al., 2007. F. Zhang, L.P. Wang, M. Brauner, J.F. Liewald, K. Kay, N. Watzke, P.G. Wood, E. Bamberg, G. Nagel, A. Gottschalk, K. Deisseroth. Multimodal fast optical interrogation of neural circuitry. *Nature,* 446 (2007), pp. 633–639

Zhang et al., 2014. J. Zhang, L.B. McKenna, C.W. Bogue, K.H. Kaestner. The diabetes gene Hhex maintains delta-cell differentiation and islet function. *Genes Dev.,* 28 (2014), pp. 829–834

Corresponding author at: Marquette University, Department of Biomedical Sciences, Milwaukee, WI 53201, United States.

The following are the supplementary data related to this article.
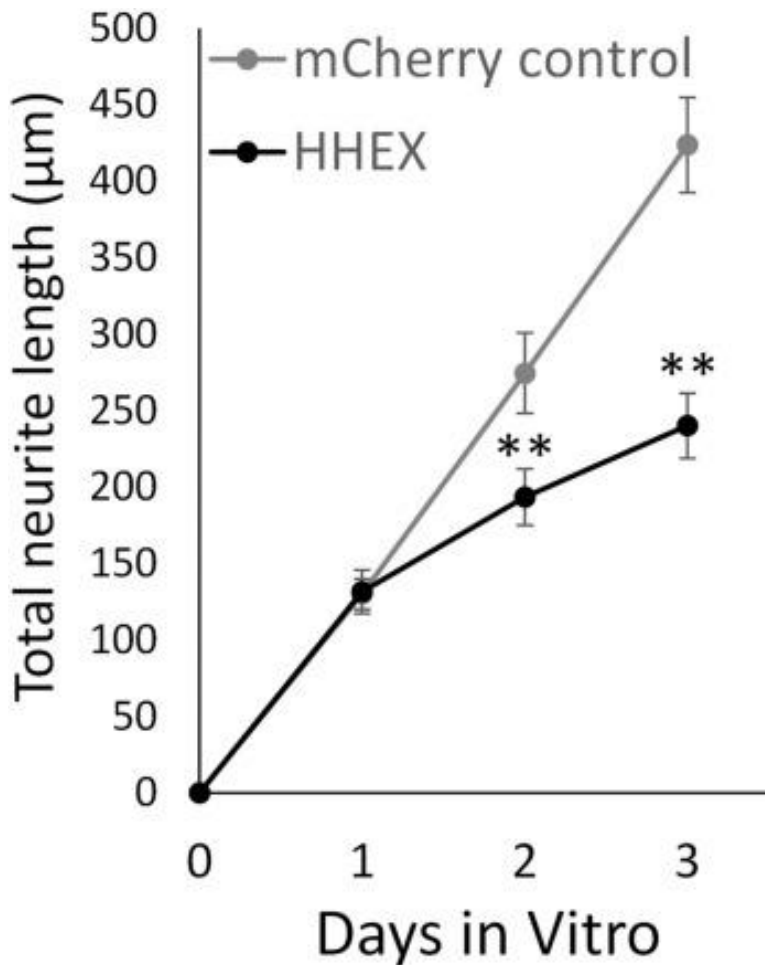
Supplemental Fig. 1. Time course analysis shows HHEX to decrease neurite extension two and three days after transfection. P3 cortical neurons were co-transfected with EGFP and either mCherry control or HHEX plasmid and cultured on laminin substrates. Cells were fixed 1, 2, or 3 days after plating, stained for neuron-specific βIII-tubulin, and total neurite outgrowth of transfected (EGFP +) neurons was quantified by automated microscopy. After a one-day period of similar outgrowth, HHEX-transfected neurons showed a reduction in neurite growth on each of the following two days. **p < .01, Paired t-test, N > 100 cells in each treatment at each time point.
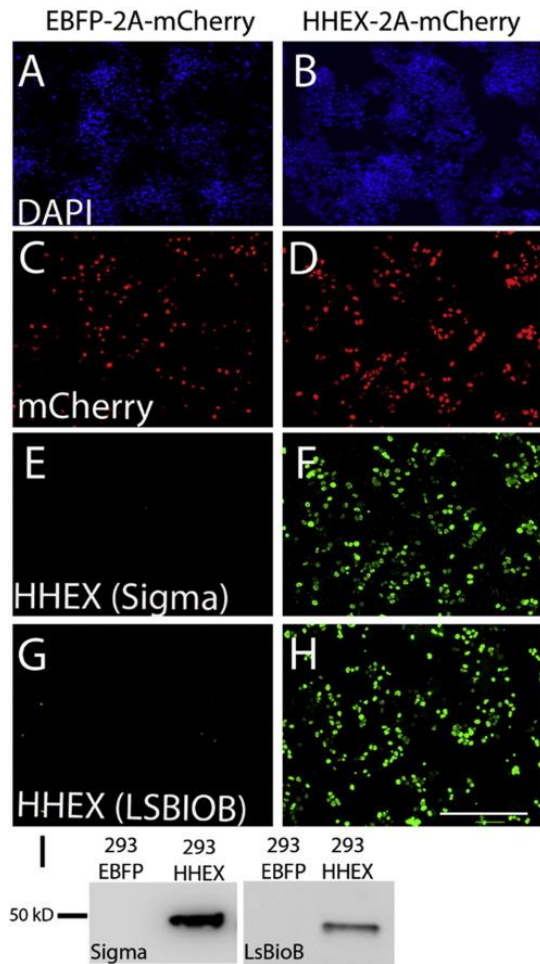
Supplemental Fig. 2. Immunohistochemistry and Western blotting confirms HHEX antibody specificity in HEK293 cells. HEK293 cells (A–H) were transfected with either EBFP-2A-H2B-mCherry or HHEX-2A-H2B-mCherry and stained with DAPI (nuclei, A and B), anti-NeuN antibodies (C,D), and two anti-HHEX antibodies (E–H). HHEX expression is detected only in cells transfected with HHEX-2A-H2B-mCherry (green, F,H). (I) Western blotting with two independent antibodies detects HHEX protein in HHEX-transfected 293 cells, but not EBFP-transfected controls. These results confirm antibody specificity. Scale bar is 100 μm.
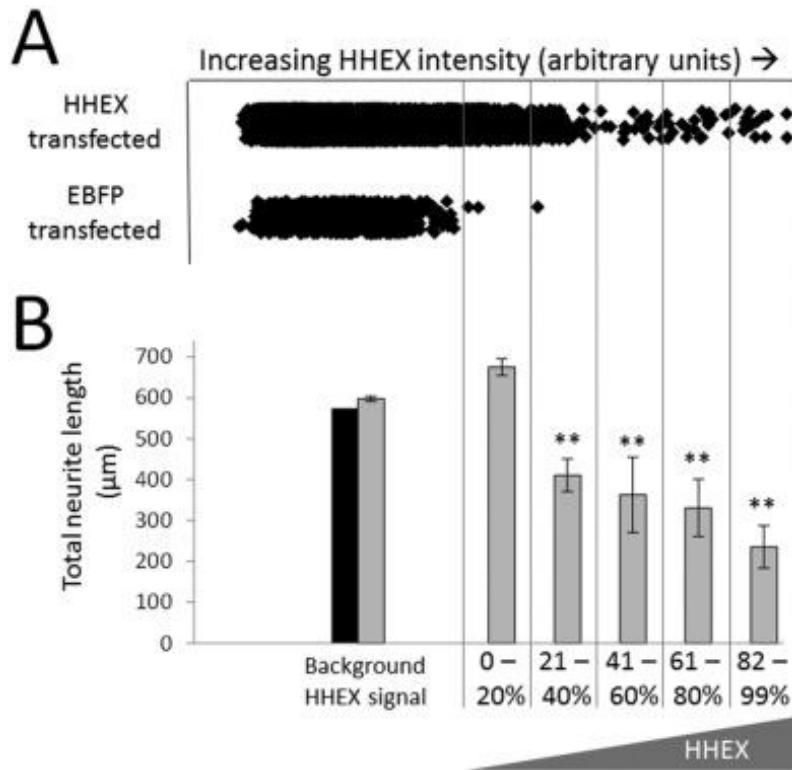
Supplemental Fig. 3. Quantitative analysis of the relationship between neurite length and level of forced HHEX protein expression. Cortical neurons were transfected with EBFP control plasmid or HHEX and maintained in culture for three days on laminin substrates. Immunohistochemistry for βIII-tubulin and HHEX protein was performed and cells were analyzed by automated microscopy (Cellomics). (A) Each dot represents the average HHEX pixel values for an individual neuron. Values within three standard deviations of the mean of EBFP-transfected cells were defined as background. As expected, HHEX overexpression resulted in numerous cells with HHEX signal above background. (B) The intensity of detection of overexpressed HHEX was divided into quintiles, and the average neurite length of neurons falling within each quintile was calculated. Significant reductions in neurite length were apparent in quintiles 2 to 5. $p < .01$, ANOVA with post-hoc Dunnet's compared to EBFP-transfected neurons. More than 10,000 total cells were analyzed.
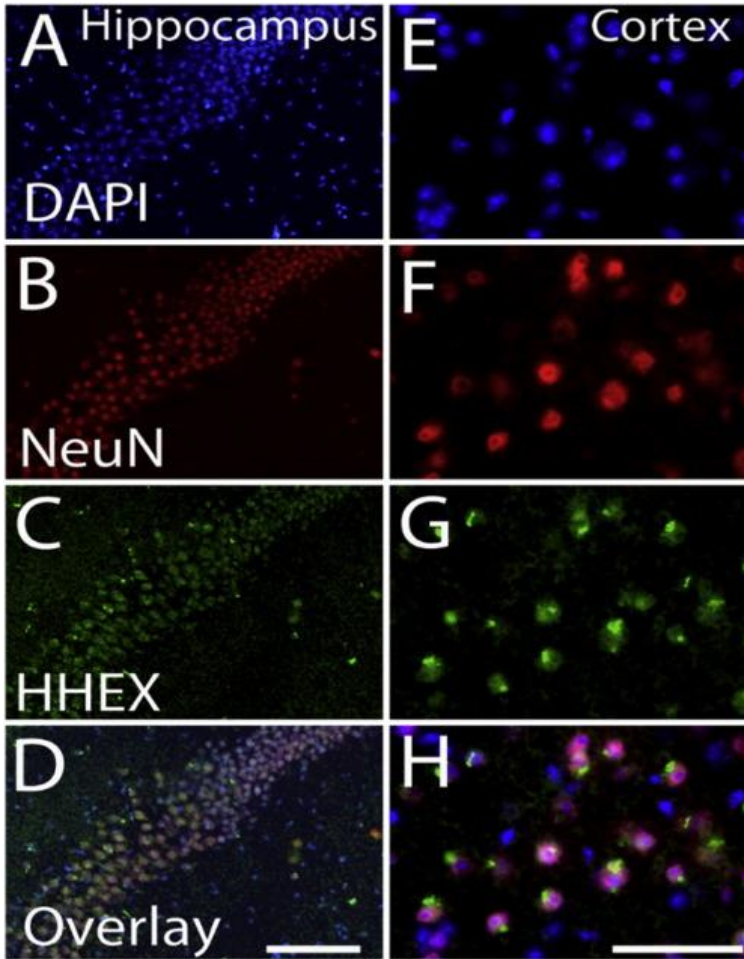
Supplemental Fig. 4. Immunohistochemistry with alternative anti-HHEX antibody confirms neuronal CNS expression. Adult mouse hippocampus (A–D) or frontal cortex (E–F) was stained with DAPI (nuclei, A and E), anti-NeuN antibodies (B,F), and anti-HHEX antibodies raised in rabbit and directed against the homeodomain region (C,G). In both hippocampus and cortex, NeuN and HHEX completely colocalized, such that HHEX was observed on only in NeuN + nuclei, and all NeuN + nuclei observed also expressed HHEX. Scale bars are 100 μm (A–D) and 50 μm (E–H).

Supplemental Table 1.

The full set of candidate genes identified as tumor suppressive or oncogenic and with predicted expression in murine cortex, along with effects on normalized neurite outgrowth in three replicate experiments.

GENE SYMBOL	Available in Open Biosystems Library?	Accession Number	Normalized Length (Expt 1)	Normalized Length (Expt 2)	Normalized Length (Expt 3)
CREB1	Human	BC010636	108.992	104.841	81.1292
CTNNB1	Human	BC058926	105.565	80.1845	91.6799
E2F1	Human	BC058902	148.574	105.063	123.16
E2F3	Human	BC016847	123.383	96.3444	124.781
EGR2	Human	BC035625	103.61	131.969	101.582
ELK1	Human	BC056150	97.7988	102.611	84.0465
ELK4	Human	BC063676	101.113	81.9492	77.1691
ERG	Human	BC040168	113.996	71.2539	82.6761
ETS2	Human	BC017040	100.695	92.7666	77.5331
ETV6	Human	BC043399	108.491	105.009	106.514
FOSB	Human	BC036724	100.56	127.844	121.274
FOSL1	Human	BC016648	120.412	106.572	101.179
HHEX	Human	BC050638	75.7829	66.2395	64.0388
HMGA1	Human	BC063434	97.1793	104.142	90.3558
HOXA5	Human	BC013682	95.1945	88.1378	91.5335
KLF4	Human	BC029923	80.0385	72.4558	67.2599
MAFB	Human	BC028098	115.889	102.236	98.5559
MAFF	Human	BC015037	104.928	77.4851	85.7434
MAX	Human	BC013669	108.317	114.895	111.951
MYC	Human	BC000917	125.409	110.345	106.459
NFKB1	Human	BC051765	87.6738	95.4123	100.993
NR4A1	Human	BC016147	92.2057	106.66	102.085
PITX1	Human	BC003685	65.5413	73.5991	81.4141
PPARG	Human	BC006811	83.5622	88.893	93.8769
RB1	Human	BC039060	88.8822	96.332	91.7567
RELA	Human	BC110830	96.5207	92.1225	89.7509
ZBTB16	Human	BC026902	78.1837	91.355	79.4925
ZFHX3	Human	BC029653	118.566	92.0885	87.93
ATF3	Mouse	BC019946	91.0746	87.146	93.9131
BCL11A	Mouse	AW22899	95.193	85.0155	108.192
BCL6	Mouse	BC052315	87.4443	95.185	105.794
CDX1	Mouse	BC019986	98.4177	112.563	105.352
CSRNP1	Mouse	BC029720	100.386	99.3558	93.814
CUX1	Mouse	BC054370	103.248	87.3118	111.604
DACH1	Mouse	BC078644	96.5486	97.0682	135.471
DDIT3	Mouse	BC013718	81.4993	86.1424	83.9582

DDX5	Mouse	BC009142	110.042	127.306	109.262
DNMT1	Mouse	BC022927	97.1934	96.9966	106.933
E2F4	Mouse	BC027030	111.296	87.4949	125.78
E2F5	Mouse	BC003220	97.8358	85.8922	90.8452
E2F6	Mouse	BC037656	101.83	96.8003	114.166
EPAS1	Mouse	BC057870	85.4695	99.3765	105.823
FOS	Mouse	AW20914	119.898	113.454	119.017
FOXO3	Mouse	BC019532	99.6987	103.514	123.721
JDP2	Mouse	BC019780	112.592	114.087	104.06
JUN	Mouse	BC002081	119.206	122.751	122.292
JUNB	Mouse	BC003790	92.6273	99.3754	95.9246
JUND	Mouse	BC023211	99.2178	89.2331	105.554
KLF6	Mouse	BC020042	115.306	134.204	128.147
MAF	Mouse	BC034073	98.3448	89.2782	99.1297
MAFG	Mouse	BC052633	99.658	90.3139	97.3636
MAFK	Mouse	BC014295	96.9112	80.9943	88.7654
MEF2C	Mouse	BC037731	104.762	106.441	125.259
MEN1	Mouse	BC036287	67.7399	106.035	113.425
MXD1	Mouse	BC023792	99.0813	98.8208	91.3152
ONECUT1	Mouse	BC024053	102.294	100.468	100.468
PML	Mouse	BC020990	97.1848	96.434	97.3713
PRDM2	Mouse	BC043456	87.2876	97.0454	85.5396
RARG	Mouse	AW76211	108.896	91.8687	102.873
RBM14	Mouse	AW76199	68.4718	65.5453	85.6647
RORA	Mouse	BC003757	88.5028	97.8821	93.2346
SKIL	Mouse	BC024908	99.6095	90.7946	106.635
STAT3	Mouse	BC019168	100.42	110.133	98.1421
TCEB3	Mouse	BC049885	94.5775	104.158	105.099
TCF4	Mouse	BC014293	93.3698	122.907	110.908
THRB	Mouse	BC042730	91.5955	84.6957	90.4564
TWIST1	Mouse	BC083139	106.147	104.772	111.197
YAP1	Mouse	BC014733	110.289	125.494	128.685
ZBTB7A	Mouse	BC024815	132.658	97.919	113.275
ABL1	Not Available				
AFF3	Not Available				
APP	Not Available				
BACH2	Not Available				
BCL11B	Not Available				
CAMTA1	Not Available				
CEBPD	Not Available				
CHD5	Not Available				
CREBBP	Not Available				
CTCF	Not Available				
DLX5	Not Available				
DMTF1	Not Available				

EGFR	Not Available
EGR1	Not Available
ENO1	Not Available
ERBB4	Not Available
ETS1	Not Available
FLI1	Not Available
FOXA1	Not Available
FOXG1	Not Available
FOXP1	Not Available
GLI1	Not Available
GLI2	Not Available
GLI3	Not Available
HBP1	Not Available
HDAC2	Not Available
HIC1	Not Available
HIF1A	Not Available
HNF4A	Not Available
HOPX	Not Available
IFI16	Not Available
IKZF3	Not Available
KLF10	Not Available
LMO4	Not Available
LZTS1	Not Available
MAPK1	Not Available
MBD2	Not Available
MXI1	Not Available
MYB	Not Available
MYBL1	Not Available
MYBL2	Not Available
MYCN	Not Available
NDN	Not Available
NFYA	Not Available
NOTCH1	Not Available
NR4A3	Not Available
OTX2	Not Available
PARP1	Not Available
PATZ1	Not Available
PAX2	Not Available
PAX6	Not Available
PAX8	Not Available
PBRM1	Not Available
PCGF2	Not Available
PDX1	Not Available
PHB	Not Available
PHOX2A	Not Available

PLAGL1	Not Available
POU6F2	Not Available
PRDM1	Not Available
PRDM4	Not Available
PRMT5	Not Available
PROX1	Not Available
RBL2	Not Available
REL	Not Available
RNF6	Not Available
RUNX2	Not Available
SAFB	Not Available
SAFB2	Not Available
SET	Not Available
SMAD4	Not Available
SMARCA2	Not Available
SMARCA4	Not Available
SMARCB1	Not Available
SMARCE1	Not Available
SOD2	Not Available
SOX4	Not Available
SOX7	Not Available
SSBP2	Not Available
SUZ12	Not Available
TCF3	Not Available
TET1	Not Available
TET2	Not Available
TFAP2A	Not Available
THRA	Not Available
TP53	Not Available
TP53BP1	Not Available
TP63	Not Available
TP73	Not Available
TSPYL2	Not Available
UBTF	Not Available
WNT1	Not Available
WNT5A	Not Available
YEATS4	Not Available
ZEB2	Not Available
ZIC1	Not Available